Research Square

Preprints are preliminary reports that have not undergone peer review.
They should not be considered conclusive, used to inform clinical practice,
or referenced by the media as validated information.

Characterizing spatiotemporal infestation cluster dynamics of two-spotted spider mite in sweet pepper screenhouses: implications for precision monitoring

Roni Gafni

roni.ga@migal.org.il

Tel Hai Academic College

Yael Edan

Ben-Gurion University of the Negev

Liran Shmuel

Agricultural Research Organization - Volcani Institute

Dana Levanon

Ben-Gurion University of the Negev

Svetlana Dobrinin

Ministry of Agriculture and Rural Development

Yafit Cohen

Agricultural Research Organization - Volcani Institute

Research Article

Keywords: Spatiotemporal dynamics, Cluster analysis, Precision pest management, Spatial monitoring, Tetranychus urticae, Screenhouse agrosystems, Pest monitoring

Posted Date: April 29th, 2026

DOI: https://doi.org/10.21203/rs.3.rs-9396303/v1

License: This work is licensed under a Creative Commons Attribution 4.0 International License.
Read Full License

Additional Declarations: No competing interests reported.

Abstract

Efficient pest monitoring in agroecosystems requires understanding fine-scale spatiotemporal infestation dynamics to enable precision management. This study characterized the field-scale spatiotemporal dynamics of the two-spotted spider mite (TSSM, *Tetranychus urticae*) in commercial sweet pepper screenhouses using a cluster-based analytical framework. Four screenhouses were monitored weekly across two growing seasons under standard regional integrated pest management practices. Infestation foci were georeferenced, and clusters were identified and tracked over time. Cluster area dynamics and directional progression relative to screenhouse boundaries were modeled across three temporal phases (*Initial*, *Rising*, *Decline*). TSSM infestations exhibited consistent spatial aggregation across seasons. Early detections were concentrated near the screenhouse perimeters, followed by mid-season expansion and late-season contraction. Cluster area increased significantly during the *Initial* and *Rising* phases (4% and 2% per day, respectively) and declined during the *Decline* phase (− 4% per day). Directional analysis revealed a preferential north–south spread during the infestation acceleration phase, aligning with crop row orientation and prevailing wind directions. This work provides the first field-based characterization of TSSM spatiotemporal dynamics in sweet pepper based on extensive, repeated sampling under commercial production conditions. Although abiotic and management variables were not explicitly modeled, the observed patterns reflect their integrated influence under commercial production conditions. These consistent spatiotemporal dynamics provide an empirical foundation for the development of spatially explicit monitoring algorithms in automated scouting systems enabling site-specific pest management.

Highlights

• A cluster-based analytical framework provided a practical basis for optimizing targeted monitoring and adaptive sampling strategies.

• Infestation foci consistently originated near screenhouse perimeters, with spatial patterns also varying among directional zones.

• Cluster dynamics followed a distinct temporal pattern, characterized by early expansion, a peak near harvest, and a subsequent decline

• Directional spread patterns revealed non-random movement of infestation clusters over time.

1. Introduction

The study of the spatial distribution of biotic stress agents is essential, as pests, diseases, and weeds commonly exhibit aggregated or patchy distributions rather than uniform patterns (Bagavathiannan and Davis 2018; Blank et al. 2023; Duarte et al. 2015). Characterizing this spatial heterogeneity is the core of site-specific management, in which control measures are applied only to infested zones instead of uniformly across entire fields (Blank et al. 2023; Méndez-Vázquez et al. 2019). Such precision-based

approaches can reduce chemical inputs by 40% to 60% (Karimzadeh and Sciarretta 2022), thereby lowering production costs and mitigating adverse environmental impacts, including groundwater contamination and the loss of non-target beneficial organisms (Duarte et al. 2015; Santos et al. 2024). Furthermore, understanding spatiotemporal dynamics of pest populations enables the development of more efficient sample strategies and robust economic thresholds, ensuring that interventions occur only when and where the probability of encountering the threat is highest (Beckler et al. 2005; Benhamouche et al. 2025; Castle and Naranjo 2009; Martins et al. 2018). In this context, translating spatiotemporal pest dynamics into actionable sampling strategies is a key component of precision pest management, particularly for spatially targeted interventions such as in the localized application of control measures or biological control agents release.

Characterizing the spatiotemporal dynamics of organisms requires intensive monitoring schemes, which are laborious, time-consuming and costly (Blank et al. 2023; Rosselo et al. 2023; Sciarretta and Trematerra 2014), hence limiting their broad adoption in commercial agroecosystems (Burgio et al. 2011; Karimzadeh and Sciarretta 2022; Sciarretta and Trematerra 2014). Robotic monitoring has the potential to reduce the time and labor costs associated with intensive in-season pest monitoring by enabling automated and adaptive crop inspection. However, their effectiveness depends not only on sensing and navigation technologies, but also on intelligent sampling strategies capable of exploiting the spatial and temporal patterns of biological targets (Oliveira et al. 2021). In this context, different algorithms that explicitly addresses the impracticality of sampling all plants in large commercial fields due to time, energy, and operational resources constraints have been proposed. Yehoshua et al. (2023) proposed a dynamic sampling algorithm that integrates prior knowledge of pest spread patterns with real-time detection data to adaptively guide sampling decisions for an agricultural monitoring ground robot. Simulation results based on real field monitoring data from commercial fields demonstrated that this strategy improves detection efficiency and reduced monitoring time, particularly in medium to large fields, compared with fixed or exhaustive sampling schemes (Yehoshua et al. 2023). Benhamouche et al. (2025) showed that smart sampling based on an ad hoc estimator that integrated model simulations with field data was 20–33% more efficient as compared to most common empirical techniques currently applied. These advances highlight the potential of moving beyond retrospective sampling approaches toward adaptive and anticipatory strategies that can prioritize locations with a higher likelihood of infestation development, provided that robust knowledge on pest spatiotemporal dynamics is available.

The two spotted spider mite (*Tetranychus urticae* Koch; hereafter TSSM) is a polyphagous parenchyma-cell feeder with more than 200 host plant species and is considered a major pest of both open-field and protected crops (Van den Boom et al. 2003). The species is characterized with a worldwide distribution (Grbić et al. 2011). The mite typically punctures the abaxial surface of leaves, causing leaf damage resulting in chlorotic discoloration and eventually leaf death (Damos et al. 2023, p. 200). TSSM development is strongly dependent on temperature and humidity, with high temperatures and low relative humidity favoring population growth (Tehri et al. 2014; Tramboo et al. 2025). Under optimal conditions of 27.5–32.5°C, the developmental period from egg to adult is completed within 7–8 days (Laing 1969). In addition, a single female may lay more than 100 eggs during its lifetime (Laing 1969).

This combination of rapid development and high fecundity renders TSSM a key pest in agroecosystems, particularly in covered vegetable crops (Tramboo et al. 2025). These biological characteristics, together with environmental and management factors, are expected to shape the spatial aggregation patterns and the temporal evolution of infestation foci within cropping systems.

TSSM populations are consistently aggregated across multiple spatial scales. At the within-leaf scale, higher TSSM abundance has been reported on the abaxial compared with the adaxial leaf surface of cucumber (Tramboo et al. 2025). At the leaf and plant level, Martínez-ferrer et al. (2006) showed that TSSM densities on citrus were higher on symptomatic leaves, suggesting that visible symptoms can serve as indicators of population dynamics. Several studies have further demonstrated preferential within-plant distribution, with TSSM tending to concentrate in the middle canopy (Alatawi et al. 2005; Tramboo et al. 2025) or the upper canopy (Chauhan and Shukla 2016), and with these patterns being influenced by the presence of predators (Walzer et al. 2009). Despite the importance of TSSM as a key agricultural pest, information on its spatiotemporal distribution at the field scale remains limited. Nachman (1981) reported near-random spatial distributions at low population densities, followed by a significant increase in aggregation as population density increased. Rijal et al. (2016) found that aggregation patches in peppermint fields extended up to approximately 7 m, with strong spatiotemporal stability evidenced by significant spatial association between most consecutive sampling dates. In protected polyhouse environment, TSSM populations exhibit distinct seasonal dynamics, characterized by phases of rapid population increase, peak abundance, and subsequent decline (Tramboo et al. 2025).

Despite these advances, a critical gap remains in the quantitative characterization of TSSM infestation dynamics at the field scale, particularly under commercial production conditions. Existing studies provide valuable insights into spatial aggregation and seasonal trends, yet they do not explicitly capture how infestation foci emerge, expand, and decline over time, nor how their location within the cropping system influences these processes. This limitation restricts the translation of observed patterns into operational decision-making. This gap is especially relevant for precision pest management, where interventions are spatially targeted. For example, biological control strategies based on localized release of predatory mites rely on the timely identification of infestation hotspots and their expected development. However, current knowledge does not sufficiently support adaptive sampling strategies that prioritize areas with a higher likelihood of infestation development, rather than relying solely on previously observed patterns.

This study aimed to characterize the spatiotemporal dynamics of TSSM in commercial sweet pepper (*Capsicum annuum*) screenhouses by tracking and analyzing infestation clusters. The overarching goal was to derive simple, interpretable rules describing cluster spatiotemporal dynamics that could guide the sampling process of automated monitoring algorithms. By linking empirical observations of infestation dynamics with potential sampling strategies, this work seeks to contribute to the development of adaptive, spatially explicit monitoring approaches in precision pest management.

2. Material and Methods

2.1. Study site

The study was conducted in Paran, located in the Arava Valley, southern Israel (30.36198°N, 35.15794°E). The region is characterized by extreme desert climatic conditions. In this area, sweet pepper is typically grown in screenhouses from late July to May. All screenhouses in this study were cultivated exclusively with sweet pepper in monoculture. Generally, screenhouses in this region are oriented in the same north–south direction and measured approximately 0.87-1 ha. A central logistic trail divided each screenhouse into northern and southern sections. Within each section, 10 construction bays (locally referred to as *gamlon*) spanned the structure. Beneath each bay, five growing beds were established, each containing two crop rows of 130 plants. This configuration resulted in approximately 26,000 plants per screenhouse. Air temperature and relative humidity (RH) were continuously monitored during both growing seasons using a HOBO U23 Pro v2 data logger (Onset Computer Corporation, Bourne, MA, USA). Measurements were recorded at 10-min intervals throughout the study period. Daily minimum and maximum air temperatures and mean daily RH were derived from these records. Daily temporal trends for both seasons are presented in the Supplementary Material (Fig. S1). Wind data were collected at 10-minute intervals from the Paran meteorological station (Israel Meteorological Service, https://ims.gov.il/he/node/237) during both growing seasons. Mean daily wind speed was calculated from hourly averages. During the study periods (July–December 2015 and 2016), mean daily maximum wind speed ranged from 4.60 to 5.76 m s^{-1} (overall mean ± SD: 5.15 ± 0.39 m s^{-1}). Wind speed showed slight seasonal variation, with higher values in the months of July–August compared to October–November. Wind direction was predominantly from the north and northeast, accounting for approximately 65% of recorded hours (Fig. S2).

In the Arava region, sweet pepper is grown under a standardized integrated pest management protocol that includes routine preventive chemical applications during the early stages of crop establishment. In the first approximately 30 days after planting, growers typically apply weekly insecticide and acaricide treatments as a prophylactic measure. Applications targeting *T. urticae* commonly include abamectin-based products, according to regional extension recommendations. After this initial period, routine chemical applications are generally discontinued unless severe pest outbreaks are detected. Upon detection of infestation foci through the weekly expert scouting scheme, growers implement localized releases of natural enemies. This protocol represents the standard commercial practice in the study area during the investigated seasons. The timing of natural enemy releases in each screenhouse relative to infestation dynamics is presented in the Supplementary Material (Fig. S3).

2.2. Sampling method

Four commercial screenhouses belonging to a single grower were sampled weekly by a human scout from September (4–5 weeks from planting) until harvest during the 2015 and 2016 growing seasons (Fig. 1). One of these screenhouses was included in both years, resulting in a total of five datasets. Table 1 provides details of the sampling events throughout the study period. During each sampling event, the scout consistently inspected the same growing bed in each bay. Within each bed, 20 plants were

selected at relatively fixed intervals along both crop rows and examined for mite presence. In subsequent weeks, in addition to inspecting 20 newly selected plants, the scout revisited plants previously identified as infested and recorded the degree of spread to neighboring plants, extending the assessment until the cluster boundary was reached. This adaptive cluster sampling method has been shown to be more effective than purely random or systematic approaches when applied to species with aggregated spatial distributions (Coggins et al. 2010). Mite population levels were determined based on visible leaf damage and supported by extension service guidelines. Infestation severity was categorized into four levels: 0 – no mites; 1 – <5 mites (low); 2–5–10 mites (medium); and 3 – >10 mites (high) (see Supplementary Material Fig. S4). This method was selected to enable a comprehensive monitoring effort while maintaining the practical feasibility of surveying two to three screenhouses in a single day.

The location of infested foci was georeferenced using a GPS–GIS device (Trimble Geo7x, CO, USA). The borders of the screenhouse were also recorded to create a polygon shapefile for each screenhouse. A point shapefile was created in which every plant was represented as a discrete spatial entity. For each sampling event, the infestation across the screenhouse was interpolated using Inverse Distance Weighting (IDW). The resulting raster surface was then sampled to the plant-level point shapefile, and the estimated infestation level was assigned to each individual plant using the *Sample Raster Values* tool in QGIS.

Table 1. Sampling dates of pepper screenhouses during the 2015–2016 growing seasons.

Growing season	Screenhouse	Planting date	Sampling dates
2015	M_4, M_11	25 Jul	09 Sep, 16 Sep, 07 Oct, 21 Oct, 28 Oct, 04 Nov, 11 Nov, 18 Nov, 25 Nov, 02 Dec, 09 Dec, 16 Dec, 23 Dec
2016	M_7, M_11, M_12	20 Jul	4 Aug, 22 Aug, 31 Aug, 04 Sep, 11 Sep, 20 Sep, 26 Sep, 06 Oct, 09 Oct, 25 Oct, 31 Oct, 07 Nov, 13 Nov, 21 Nov, 28 Nov

2.3. Exploratory analysis of spatiotemporal infestation patterns

The dataset was examined to identify potential spatial or temporal dependencies. The temporal trends of infested points (Infestation severity > 0) were calculated by days after planting (DAP) for each year for each screenhouse (Fig. S5). To enable spatial comparison among screenhouses located at different geographical positions, spatial coordinates were normalized using min-max scaling. For each screenhouse, X and Y coordinates were transformed to a 0-100% scale, where 0% and 100% represented the minimum and maximum coordinate values within each screenhouse boundary, respectively. This normalization allowed for direct comparison of spatial infestation patterns across screenhouses regardless of their absolute geographic locations (Supplementary data, Figure S6). As visual inspection

of the data revealed no trends attributable to a specific year or screenhouse, all screenhouses were included in the subsequent spatiotemporal analyses.

Spatial aggregation was quantified using the Average Nearest Neighbor Index (ANN). The ANN was calculated for each sampling event in each screenhouse throughout the growing season as the ratio between the observed mean nearest-neighbor distance among infested plants and the expected mean distance under complete spatial randomness. Values significantly lower than 1 indicate aggregated spatial patterns. For each screenhouse, buffer zones were generated at 10 m intervals up to 30 m from the screenhouse edge. These buffers were used to calculate the proportion of infested points in each severity category as a function of distance from the edge.

2.4. Spatiotemporal analysis of infestation cluster dynamics

2.4.1. Overview

To characterize the spatiotemporal dynamics of TSSM infestations, a structured sequence of spatial and temporal processing steps was applied to the georeferenced sampling dataset. The workflow integrated spatial clustering, temporal classification, and directional movement analysis to quantify cluster initiation, expansion, and contraction throughout the growing season. The main analytical steps were:

[1] Cluster identification: Infested sampling points were grouped into spatial clusters representing infestation foci.

[2] Cluster origin analysis: Each screenhouse was divided into four quadrants (NE, NW, SE, SW) to examine spatial patterns in cluster initiation.

[3] Temporal phase classification: Sampling events were categorized into *Initial*, *Rising*, and *Decline* phases based on overall infestation trends.

[4] Directional spread analysis: Cluster expansion rates and movement directions were quantified to assess preferential spread patterns across infestation phases.

Detailed description of each step is provided in the following sections. All spatial and statistical analyses were conducted in R (R Core Team 2022), with visualization performed using the 'ggplot2' package (Wickham 2011).

2.4.2 Cluster identification

Since the objective of this analysis was to detect the presence and spatial grouping of mite infestations rather than quantify intensity, observations were simplified into two classes: 0 – no mites detected and 1 – mites detected; infestation intensity levels were not considered.

Mite infestation clusters were identified using the density-based spatial clustering method (DBSCAN; Ester et al. 1996) with parameters *eps* = 2 and *minPts* = 2. This approach grouped spatially proximate infestation points while excluding isolated detections. For each sampling date, clusters boundaries were delineated by buffering the union of clustered points by one m.

A cluster-tracking algorithm was developed to track infestation progress over time. Clusters were assigned persistent identification numbers based on spatial overlap between consecutive sampling events. A cluster was assigned the identification number of a cluster from the previous sampling date if spatial intersected occurred within a 2 m buffer tolerance. Clusters without spatial correspondence to prior detections were designated as new and assigned unique identification numbers (Fig. 2). This step formed the basis for analyzing how localized infestations develop and propagate within the screenhouse.

2.4.3 Cluster origin

To evaluate potential directional patterns in infestation spread, each screenhouse was partitioned into four quadrants (Northeast, Northwest, Southeast, Southwest). This division was motivated by observed edge effects and the need to determine whether infestations preferentially originated from specific directions or entry points. The quadrants were defined by connecting the geometric midpoints of each screenhouse wall to the centroid, thereby creating four spatially comparable sections. This standardized framework enabled consistent assessment of infestation distributions relative to cardinal directions across screenhouses of varying shapes and sizes. Each cluster was subsequently assigned to its quadrant of origin (NE, NW, SE, SW), enabling evaluation of whether sampling efforts could be spatially prioritized.

2.4.4. Temporal phase classification

For each year, the total infested area per day was summed across all screenhouses and slope values (change in area per day) were calculated (Figure S7). Absolute and relative slope values were then derived to quantify the magnitude and direction of infestation growth or decline. Based on these metrics, three temporal phases were identified: (1) *Initial* – characterized by a positive but low relative slope (< 10%) and small total area (< 10% of the annual maximum); (2) *Rising* – total area > 10% of the maximum with a positive slope; and (3) *Decline* – negative slope occurring after the maximum total area was reached. Median transition points between phases of both years were used to establish general phase boundaries at 75 and 100 DAP. This classification enabled comparison of infestation dynamics across distinct temporal stages.

2.4.5. Directional spread analysis

To analyze cluster progression throughout the season, spatial relationships between infestation clusters and the screenhouse boundaries were quantified by measuring the shortest distance from each cluster polygon to the northern, southern, eastern, and western walls at each sampling date. For clusters detected on more than three consecutive sampling dates, temporal changes in position were estimated

using a linear regression model, with distance as the response variable and DAP as the predictor. The resulting slope coefficients quantified both rate and direction of movement; negative slopes indicated progression towards a given wall, whereas positive slopes reflected movement away from it.

This approach enabled quantitative assessment of cluster displacement over time in terms of both direction and magnitude. Clusters were classified as 'advancing' when the absolute slope values exceeded 0.1, corresponding to a distance change rate greater than 10 cm day^{-1}, and as 'static' when the absolute slope was ≤ 0.1. Clusters lacking sufficient temporal observations for slope estimation were categorized as single observations. This classification framework allowed evaluation of whether cluster expansion exhibits consistent directional tendencies.

2.4.6. Statistical analysis

To examine whether the spatial origin of infestation clusters varies across temporal phases, a heatmap summarizing the number of clusters originating from each screenhouse quadrant across temporal phases was generated. Statistical associations between the initial section of cluster formation and temporal phase were tested using Fisher's exact test ($\alpha = 0.05$).

To assess temporal changes in cluster area within each phase, cluster area was modeled as a function of DAP. As very large clusters are easily detected and typically trigger pesticide treatments over the entire plot, the dataset was filtered to include only clusters with an area smaller than 100 m² along more than two consecutive observations. Generalized Linear Mixed Models (GLMM) with a Gamma distribution and log link function were fitted separately for each phase using the 'glmmTMB' package (Brooks et al. 2017). Cluster area was included as the response variable, DAP as the fixed explanatory variable, and cluster identity nested within screenhouse as a random effect, to account for repeated measurements of the same cluster over time. Estimated marginal means were obtained using the 'emmeans' package (Lenth 2022) with pairwise comparisons conducted using Tukey's adjustment ($\alpha = 0.05$).

To evaluate directional patterns of cluster movement and differences in spread rates among directions and temporal phases, summary statistics of slope values (mean and standard deviation) were calculated for each direction and phase (Table S1). Clusters advancing toward a given direction were subsequently analyzed using Generalized Additive Models for Location, Scale, and Shape (GAMLSS) with a Power Exponential (PE) distribution, accommodating deviations from normality. Models were fitted using the 'gamlss' package (Rigby and Stasinopoulos 2005).

Analyses were limited to the *Rising* and *Decline* phases due to the small number of advancing clusters observed during the *Initial* phase. For each temporal phase, slope was specified as the response variable and direction as the explanatory variable, with screenhouse treated as a random effect. To account for heteroscedasticity, a separate sigma model incorporating direction as a covariate was fitted. Estimated marginal means were calculated using the 'emmeans' package (Lenth 2022) for each direction within each phase, and pairwise comparisons were conducted using Tukey's adjustment ($\alpha = 0.05$).

3. Results

3.1. Spatiotemporal patterns of infestation

Across all sampling events, screenhouses, and growing seasons, the ANN index was consistently and significantly lower than 1 (Table S2), indicating a non-random, aggregated spatial distribution of TSSM infestations.

Mite detections exhibited a consistent temporal pattern across screenhouses, characterized by an early rise in infested points, a peak coinciding with the onset of harvest, and a gradual decline during the winter months. Figure 3 illustrates the distribution of infestation foci throughout the growing season across distance zones from the screenhouse edges and among severity levels. Infestation onset occurred earlier near the screenhouse walls: low- and medium-severity foci were detected as early as 30 DAP within 20 m of the screenhouse perimeter, whereas comparable detections in the central zone (> 30 m from the edge) appeared later, around 60–80 DAP. Peak infestation coincided with the onset of harvest (70–110 DAP), with medium-severity foci exhibiting sharper and more pronounced peaks than low-severity detections. High-severity foci emerged mainly between 70 and 110 DAP and accounted for only a small proportion of total observations. Overall, the earliest occurrences and highest infestation levels were consistently concentrated near the screenhouse perimeter, within the 0–10 m zone.

3.2. Cluster formation and spatiotemporal distribution

Analysis of the initial section of cluster formation (Fig. 4) showed no statistically significant association between the quadrant of first appearance and temporal phase (Fisher's exact test, $p = 0.223$). Nevertheless, several spatial tendencies were apparent. During the *Initial* phase, most clusters originated in the northern sections (18 and 12 in the NE and NW, respectively), with fewer forming in the southern quadrants (7 and 3 in the SE and SW, respectively). In the *Rising* phase, the overall number of clusters was highest, with new clusters emerging across all sections. However, cluster formation was more pronounced in the western quadrants, with 11 and 14 new clusters formed in the NW and SW quadrants, respectively, compared to 6 and 9 new clusters formed in the NE and SE quadrants, respectively. In the *Decline* phase, cluster formation was more evenly distributed, though slightly elevated in the SE section.

3.3. Cluster growth analysis

Figure 5 illustrates the change in area of individual clusters throughout the growing season. Of the 124 clusters identified, 17 exceeded an area of 100 m^2 and were therefore excluded from subsequent area-based analysis. Modeling cluster area as a function of DAP revealed phase-dependent dynamics (Table 2). During the *Initial* and *Rising* phases, cluster area increased significantly over time, at estimated rates of 4% and 2% per day, respectively. In contrast, cluster area decreased significantly during the *Decline* phase at an estimated rate of 4% per day. The mean cluster area at the onset of the *Rising* phase

was approximately 12 m², increasing to approximately 22 m² at the seasonal peak preceding the *Decline* phase (Table 2).

Table 2
Results of generalized linear mixed models describing the relationship between TSSM infestation cluster area and Days After Planting (DAP) across temporal phases (*Initial*, *Rising*, and *Decline*). Coefficient estimates describe proportional changes in cluster area over time, with positive and negative DAP coefficients indicate increases and decreases in cluster area, respectively. Estimated mean responses and corresponding confidence intervals (CI) are presented.

Temporal phase	Term	Estimate ± SE	P value	Estimated Response	CI
Initial	DAP	0.04 ± 0.003	< 2e-16 ***	1.04	[1.03, 1.05]
Rising	Intercept	2.49 ± 0.16	< 2e-16 ***	12.0 m^2	[8.8, 16.5]
	DAP	0.02 ± 0.008	0.0168 *	1.02	[1.003, 1.035]
Decline	Intercept	3.09 ± 0.12	< 2e-16 ***	21.9 m^2	[17.4, 27.6]
	DAP	-0.04 ± 0.005	< 2e-16 ***	0.96	[0.95, 0.97]

3.4. Cluster directional progression

Mean slope values were negative in all directions during the *Initial* and *Rising* phases, while mean slopes during the *Decline* phase were positive across all directions (Fig. 6). Table 3 summarizes the mean directional trends estimated from models fitted to the *Rising* and *Decline* phases. During the *Rising* phase, the highest movement rate was observed toward the southern boundary (0.57 m day^{-1}), followed by the northern boundary (0.37 m day^{-1}), while the lowest rate occurred toward the eastern boundary (Table 3). During the *Decline* phase, slopes were positive in all directions, with similar rates of increase in distance from the northern and southern boundaries, slightly lower rates from the western boundary, and the lowest rate from the eastern boundary (Table 3).

Table 3
Estimated mean rates of change in distance between TSSM infestation clusters and the screenhouse boundaries during the *Rising* and *Decline* temporal phases. Values represent mean slope estimates (m day^{-1}) for each cardinal direction (North, South, East, and West), with positive values indicating increasing distance from the boundary and negative values indicating decreasing distance. Confidence intervals are shown for each estimate.

Temporal phase	**Direction**	**Estimate Response (m day^{-1})**	**CI**
Rising	North	-0.371	[-0.374,-0.367]
	South	-0.573	[-0.576,-0.570]
	East	-0.171	[-0.173,-0.169]
	West	-0.229	[-0.230,-0.227]
Decline	North	0.286	[0.285, 0.287]
	South	0.286	[0.284, 0.287]
	East	0.139	[0.137, 0.141]
	West	0.229	[0.228, 0.230]

4. Discussion

Cluster-based analysis of TSSM spatiotemporal dynamics in commercial sweet pepper screenhouses revealed consistent spatial aggregation, phase-dependent changes in cluster area, and directional movement patterns throughout the first half of the growing season. The aggregation pattern observed here corresponds with previous reports of within-field TSSM aggregation in diverse cropping systems, including roses (So 1991), open-field peppermint (Rijal et al. 2016), greenhouse-grown and open-field strawberry (Greco et al. 2004; Greco et al. 1999), and glasshouses-grown cucumber (Nachman 1981).

Previous investigations of TSSM spatial distribution have primarily focused on predator–prey interactions or have relied on laboratory experiments and models based on global population metrics, such as mean density or the proportion of infested plants (Greco et al. 2004; Kozlova et al. 2005; Nachman 1981; Sabelis et al. 2005). The extensive and repeated field sampling conducted under commercial conditions enabled a fine-scale characterization of cluster initiation, expansion, and directional spread. This approach revealed consistent spatiotemporal tendencies that can inform practical monitoring strategies and support the development of rule-based automated scouting algorithms.

In this study, TSSM population dynamics on sweet pepper grown in screenhouses followed a characteristic seasonal trajectory, consisting of early expansion, peak during the beginning of harvest,

and a gradual decline toward the winter months. A similar temporal pattern was reported by Tramboo et al. (2025) in cucumber cultivated under polyhouse conditions, where population increases were associated with vigorous vegetative growth and declines were linked to plant senescence. Comparable dynamics have also been documented for TSSM on field-grown cucumber (Tehri et al. 2014), corn and peanuts (Margolies and Kennedy 1985), and brinjal (Patidar et al. 2023).

Several studies further associated these population trends with abiotic conditions. Chauhan and Shukla (2016) reported a positive correlation between TSSM density and maximum temperature in French beans grown under polyhouse conditions, while Patidar et al. (2023) found a positive relationship with maximum temperature and a negative relationship with relative humidity.

At the beginning of the growing season, abiotic conditions in the commercial screenhouses were highly favorable for TSSM development, with mean daily temperature and relative humidity of 33.2 ± 1.4°C and 36.0 ± 7.0%, respectively. Accordingly, regional management practices typically involve weekly chemical applications during the first 30 days after planting, and mite infestations are usually detected only after these applications are discontinued.

During the *Initial* phase (up to 75 DAP), mean temperatures were slightly lower (30.3 ± 1.9°C) and mean relative humidity higher (43.6 ± 7.4%), yet environmental conditions remained within the optimal range for TSSM development (Damos et al. 2023). In the *Rising* phase (75–100 DAP), temperatures declined further (25.1 ± 2.5°C) while relative humidity increased (55.3 ± 12.4%). Despite these comparatively less favorable conditions, the total infested area continued to expand, with dozens of infestation foci growing from initial sizes of approximately 9–16 m². Although the rate of expansion was lower than during the *Initial* phase, population growth persisted, likely reflecting cumulative generational effects, as suggested by Damos et al. (2023).

In contrast, during the *Decline* phase, mean temperature and relative humidity reached 16.2 ± 4.5°C and 54.5 ± 8.8%, respectively, conditions no longer favorable for TSSM development (Tehri et al. 2014; Tramboo et al. 2025). These environmental conditions align with the observed contraction and eventual disappearance of infestation clusters.

Mite infestations frequently originate at field margins (Margolies and Kennedy 1985). In line with this pattern, TSSM foci in this study were first detected near screenhouse edges, underscoring the importance of concentrating monitoring efforts along the perimeter during the *Initial* phase. This spatial tendency should be considered when designing monitoring algorithms for automated scouting systems. Similarly, Rijal et al. (2016) emphasized the effectiveness of early-season edge sampling when combined with systematic sampling.

Analysis of the contribution of screenhouse sections to cluster formation did not reveal a statistically significant association between quadrant of origin and temporal phase. Nevertheless, a weak but consistent spatial tendency emerged: early infestations were more likely to originate in the northern rather than southern sections, and in the eastern rather than western sections of the screenhouse. The

NE and NW sections contributed relatively high numbers of new clusters during the *Initial* phase, but their contribution declined in later phases. In contrast, the western sections (NW and SW) exhibited a marked increase in new cluster formation during the *Rising* phase, suggesting that as the epidemic intensified, new infestation foci were more likely to emerge in these areas. These patterns indicate a spatial bias in early season cluster emergence within the screenhouse. It is important to note that this analysis characterizes the spatial distribution of cluster initiation sites and does not track the persistence of individual clusters across temporal phases.

Nachman (1981) reported recurring patterns of TSSM outbreak occurrence in cucumber across three glasshouse systems, with infestations appearing first in south-facing structures, followed by east- and west-facing systems, and finally in north-facing systems. These differences were attributed to microclimatic variation among glasshouses. Similarly, the spatial patterns of cluster initiation observed in the present study may reflect microclimatic heterogeneity within the screenhouse environment. Temperature and relative humidity data collected during the 2016 season indicated minor but consistent differences among screenhouse sections, with the northern section being marginally warmer during the *Initial* phase (by approximately 0.5°C; data not shown). These findings highlight the importance of interpreting pest dynamics within the context of local production systems rather than relying solely on general rules. Nevertheless, both studies suggest that systematic spatial tendencies can emerge at broader regional scales, despite local microclimatic differences. Although abiotic conditions and management interventions were not explicitly modeled, the cluster dynamics described here likely represent the integrated outcome of these interacting factors under a commercial production system.

Temporal phases in this study were defined based on system-level trends in total infested area aggregated across screenhouses within each growing season, whereas cluster growth and directional dynamics were analyzed independently at the individual cluster level. The cluster-based analysis revealed phase-specific directional patterns of infestation spread. During the *Initial* and *Rising* phases, slopes were negative across all directions, indicating expansion toward the screenhouse boundaries. In contrast, mean slopes during the *Decline* phase were positive in all directions, reflecting movement away from the boundaries and overall contraction of infestation clusters. The model fitted for the *Rising* phase indicated preferential spread from north to south, aligned with crop row orientation. Although not formally modeled for the *Initial* phase, a similar tendency was evident: most clusters were classified as 'advancing' toward the northern and southern borders but 'static' toward the eastern and western borders (Supplementary Table S1). Consequently, eastern movement exhibited the lowest estimated rate during the *Rising* phase. The tendency for clusters to originate near the northern and eastern borders may partially explain these directional dynamics.

TSSM dispersal occurs primarily through ambulatory movement along interconnected leaves or plants or structural elements (Nachman 1987), as well as through aerial dispersal when local conditions deteriorate due to declining host quality (Meck et al. 2009), intraspecific competition (Bitume et al. 2013; Li and Margolies 1993), or predation pressure (Croft and Jung 2001; Nachman 1981). Aerial dispersal carries substantial mortality risk when mites land in unsuitable environments (Boykin and Campbell

1984). Under laboratory conditions, adult females have been shown to walk distances of up to 4.8 m (Krainacker and Carey 1990). Croft and Jung (2001) reported that *Neoseiulus fallacis*, a phytoseiid predator of TSSM, can disperse by wind over distances of up to 100 m, depending on crop height and architecture; however, these observations were made in open-field agroecosystems. While wind-mediated dispersal is generally considered negligible in enclosed greenhouses (Zemek and Nachman 1999), the net-covered structure of the screenhouses in the present study may allow some wind influence. The higher rate of spread toward the southern border may therefore reflect the north–south orientation of crop rows, prevailing northerly winds during the *Initial* and *Rising* phases (Fig. S2), or a combination of both factors.

The results of this study extend current understanding of TSSM dynamics by shifting the focus from static descriptions of spatial aggregation toward the characterization of infestation foci as dynamic entities that evolve over time, thereby enabling their quantitative analysis. Unlike previous studies that primarily relied on mean density measures or the proportion of infested plants, this approach captures both the spatial structure and temporal progression of infestations at a finer operational scale. The consistent spatiotemporal patterns identified here, including early emergence near field margins and phase-dependent directional spread, suggest that cluster dynamics may provide a valuable basis for precision monitoring approaches, particularly in production systems where localized interventions are required.

5. Conclusion and implications for pest monitoring

This study demonstrates that TSSM infestations in commercial sweet pepper screenhouses exhibit consistent spatial aggregation, phase-dependent dynamics, and directional spread patterns. The observed clustering distribution observed across growing seasons supports the implementation of data-driven, site-specific pest monitoring strategies. To our knowledge, this work represents the first field-based characterization of TSSM spatiotemporal dynamics in sweet pepper derived from extensive, repeated sampling under commercial production conditions.

The phase-specific spatial tendencies identified here can inform practical monitoring guidelines: early-season inspections should prioritize the northern and eastern screenhouse perimeters, monitoring during infestation acceleration should align with crop rows and prevailing wind direction to capture preferential north–south spread, and sampling intensity may be adaptively reduced during late-season contraction. The empirical rules derived from multiple clusters across locations and seasons provide a foundation for spatially explicit modeling frameworks, including cellular automata and other rule-based approaches. This may support the development of automated scouting and adaptive monitoring systems, enabling site-specific pest management.

These findings should be interpreted within the context of the studied production system, characterized by extreme desert conditions and a defined regional pest management protocol. While specific spatial

biases may vary across systems, the broader principles of aggregation and phase-structured dynamics are likely transferable to other protected cropping environments.

Declarations

Conflict of interest

The authors declare that they have no competing interests.

Use of Artificial Intelligence

During manuscript preparation, the authors used ChatGPT (OpenAI) and Claude (Anthropic) to assist with language editing, text refinement, and improvement of clarity and structure. The AI tool was not used for data analysis, interpretation of results, or generation of scientific content beyond linguistic and editorial support. All scientific content, analyses, and conclusions were developed and verified by the authors.

Funding

This research was funded by the Chief Scientist, Israel Ministry of Agriculture and Food Security (Grant No. 16-29-0004).

Author Contribution

R.G. developed the methodology, performed the statistical analysis, and wrote the original draft of the manuscript. Y.E. and Y.C. secured funding, conceptualized the experimental design and analyses methodology, and reviewed and edited the analyses and manuscript through to its final version. L.S. conducted data curation and collected the data. D.L. contributed to the study concept and assisted with statistical analysis, particularly the definition of temporal phases. S.D. contributed to data curation and developed the mite sampling strategy. All authors reviewed and approved the final manuscript

Acknowledgement

The authors would like to thank the growers of Margal Corporation, Paran, for their cooperation and for granting access to the commercial screenhouses. We are grateful to the professional pest scout Leonid Dobrinin for his assistance and for sharing his monitoring records. We also thank Eitan Goldstein for his valuable support.

Data Availability

The datasets analyzed and the scripts used during the current study are available from the corresponding author upon justified request.

References

1. Alatawi, F. J., Opit, G. P., Margolies, D. C., & Nechols, J. R. (2005). Within-plant distribution of twospotted spider mites (Acari: Tetranychidae) on impatiens: development of a presence–absence sampling plan. *Journal of Economic Entomology*, *98*(3), 1040–1047. https://doi.org/10.1603/0022-0493-98.3.1040
2. Bagavathiannan, M. V., & Davis, A. S. (2018). An ecological perspective on managing weeds during the great selection for herbicide resistance. *Pest Management Science*, *74*(10), 2277–2286. https://doi.org/10.1002/ps.4920
3. Beckler, A. A., French, W., B., & Chandler, L. D. (2005). Using GIS in areawide pest management: A case study in South Dakota. *Transactions in GIS*, *9*(2), 109–127. https://doi.org/10.1111/j.1467-9671.2005.00209.x
4. Benhamouche, O., Rossini, L., Rosselló, N. B., Pezzutto, M., Turco, S., & Garone, E. (2025). A win–win combination in plant disease prediction: field data to update model estimations, estimations to drive field data collection. *European Journal of Plant Pathology*. https://doi.org/10.1007/s10658-025-03166-2
5. Bitume, E. V., Bonte, D., Ronce, O., Bach, F., Flaven, E., Olivieri, I., & Nieberding, C. M. (2013). Density and genetic relatedness increase dispersal distance in a subsocial organism. *Ecology Letters*, *16*(4), 430–437. https://doi.org/10.1111/ele.12057
6. Blank, L., Rozenberg, G., & Gafni, R. (2023). Spatial and temporal aspects of weeds distribution within agricultural fields – A review. *Crop Protection*, *172*, 106300. https://doi.org/10.1016/j.cropro.2023.106300
7. Boykin, L. S., & Campbell, W. V. (1984). Wind dispersal of the twospotted spider mite (Acari: Tetranychidae) in North Carolina peanut fields. *Environmental Entomology*, *13*(1), 221–227. https://doi.org/10.1093/ee/13.1.221
8. Brooks, M., Kristensen, E., van Benthem, K., Magnusson, K. J., Berg, A., Nielsen, C. W., A., et al. (2017). glmmTMB balances speed and flexibility among packages for zero-inflated generalized linear mixed modeling. *The R Journal*, *9*(2), 378. https://doi.org/10.32614/RJ-2017-066
9. Burgio, G., Ragaglini, G., Petacchi, R., Ferrari, R., Pozzati, M., & Furlan, L. (2011). Optimization of *Agriotes sordidus* monitoring in northern Italy rural landscape, using a spatial approach. *Bull Insectology*, *65*.
10. Castle, S., & Naranjo, S. E. (2009). Sampling plans, selective insecticides and sustainability: the case for IPM as informed pest management. *Pest Management Science*, *65*(12), 1321–1328. https://doi.org/10.1002/ps.1857

11. Chauhan, R. K., & Shukla, A. (2016). Population dynamics of two spotted spider mite, *Tetranychus urticae* Koch on French bean (*Phaseolus vulgaris* L). *International Journal of Plant Protection*, *9*(2), 536–539. https://doi.org/10.15740/HAS/IJPP/9.2/536-539
12. Coggins, S. B., Coops, N. C., & Wulder, M. A. (2010). Estimates of bark beetle infestation expansion factors with adaptive cluster sampling. *International Journal of Pest Management*, *57*(1), 11–21. https://doi.org/10.1080/09670874.2010.505667
13. Croft, B. A., & Jung, C. (2001). Phytoseiid dispersal at plant to regional levels: a review with emphasis on management of *Neoseiulus fallacis* in diverse agroecosystems. *Experimental & Applied Acarology*, *25*(10), 763–784. https://doi.org/10.1023/A:1020406404509
14. Damos, P., Papathanasiou, F., Tsikos, E., Kyriakidis, T., & Louta, M. (2023). Predicting the occurrence and risk damage caused by the two-spotted spider mite *Tetranychus urticae* (Koch) in dry beans (*Phaseolus vulgaris* L.) combining rate and heat summation models for digital decisions support. *Agriculture*, *13*(4), 756. https://doi.org/10.3390/agriculture13040756
15. Duarte, F., Calvo, M., Borges, A., & Scatoni, I. (2015). Geostatistics applied to the study of the spatial distribution of insects and its use in integrated pest management. *Revista Agronomica del Noroeste Argentino*, *35*, 9–20.
16. Ester, M., Kriegel, H. P., Sander, J., & Xu, X. (1996). A density-based algorithm for discovering clusters in large spatial databases with noise. In *Proceedings of the Second International Conference on Knowledge Discovery and Data Mining* (pp. 226–231). Portland, Oregon: AAAI Press. Accessed 20 April 2025.
17. Grbić, M., Van Leeuwen, T., Clark, R. M., Rombauts, S., Rouzé, P., Grbić, V., et al. (2011). The genome of < I>Tetranychus urticae reveals herbivorous pest adaptations. *Nature*, *479*(7374), 487–492. https://doi.org/10.1038/nature10640
18. Greco, N. M., Liljeström, G. G., & Sánchez, N. E. (1999). Spatial distribution and coincidence of *Neoseiulus californicus* and *Tetranychus urticae* (Acari: Phytoseiidae, Tetranychidae) on strawberry. *Experimental & Applied Acarology*, *23*(7), 567–579. https://doi.org/10.1023/A:1006125103981
19. Greco, N. M., Tetzlaff, G. T., & Liljesthröm, G. G. (2004). Presence–absence sampling for *Tetranychus urticae* and its predator *Neoseiulus californicus* (Acari: Tetranychidae; Phytoseiidae) on strawberries. *International Journal of Pest Management*, *50*(1), 23–27. https://doi.org/10.1080/09670870310001626338
20. Karimzadeh, R., & Sciarretta, A. (2022). Spatial patchiness and association of pests and natural enemies in agro-ecosystems and their application in precision pest management: a review. *Precision Agriculture*, *23*(5), 1836–1855. https://doi.org/10.1007/s11119-022-09902-6
21. Kozlova, I., Singh, M., Easton, A., & Ridland, P. (2005). Twospotted spider mite predator-prey model. *Mathematical and Computer Modelling*, *42*(11), 1287–1298. https://doi.org/10.1016/j.mcm.2005.01.036
22. Krainacker, D. A., & Carey, J. R. (1990). Ambulatory dispersal and life history response to food deprivation in twospotted spider mites. *Entomologia Experimentalis et Applicata*, *56*(2), 139–144.

https://doi.org/10.1111/j.1570-7458.1990.tb01391.x

23. Laing, J. E. (1969). Life history and life table of *Tetranychus urticae*. *Acarologia*, *11*(1), 32–42.
24. Lenth, R. V. (2022). emmeans: Estimated Marginal Means, aka Least-Squares Means. https://CRAN.R-project.org/package=emmeans
25. Li, J., & Margolies, D. C. (1993). Effects of mite age, mite density, and host quality on aerial dispersal behavior in the twospotted spider mite. *Entomologia Experimentalis et Applicata*, *68*(1), 79–86. https://doi.org/10.1111/j.1570-7458.1993.tb01691.x
26. Margolies, D. C., & Kennedy, G. G. (1985). Movement of the twospotted spider mite, *Tetranychus urticae*, among hosts in a corn-peanut agroecosystem. *Entomologia Experimentalis et Applicata*, *37*(1), 55–61. https://doi.org/10.1111/j.1570-7458.1985.tb03452.x
27. Martínez-Ferrer, M. T., Jacas, J. A., Ripollés-Moles, J. L., & Aucejo-Romero, S. (2006). Approaches for sampling the twospotted spider mite (Acari: Tetranychidae) on clementines in Spain. *Journal of Economic Entomology*, *99*(4), 1490–1499. https://doi.org/10.1093/jee/99.4.1490
28. Martins, J. C., Picanço, M. C., Silva, R. S., Gonring, A. H., Galdino, T. V., & Guedes, R. N. (2018). Assessing the spatial distribution of *Tuta absoluta* (Lepidoptera: Gelechiidae) eggs in open-field tomato cultivation through geostatistical analysis. *Pest Management Science*, *74*(1), 30–36. https://doi.org/10.1002/ps.4664
29. Meck, E. D., Walgenbach, J. F., & Kennedy, G. G. (2009). Effect of vegetation management on autumn dispersal of *Tetranychus urticae* (Acari: Tetranychidae) from tomato. *Journal of Applied Entomology*, *133*(9–10), 742–748. https://doi.org/10.1111/j.1439-0418.2009.01413.x
30. Méndez-Vázquez, L. J., Lira-Noriega, A., Lasa-Covarrubias, R., & Cerdeira-Estrada, S. (2019). Delineation of site-specific management zones for pest control purposes: Exploring precision agriculture and species distribution modeling approaches. *Computers and Electronics in Agriculture*, *167*, 105101. https://doi.org/10.1016/j.compag.2019.105101
31. Nachman, G. (1981). Temporal and spatial dynamics of an acarine predator-prey system. *Journal of Animal Ecology*, *50*(2), 435–451. https://doi.org/10.2307/4065
32. Nachman, G. (1987). Systems analysis of acarine predator-prey interactions. I. A stochastic simulation model of spatial processes. *Journal of Animal Ecology*, *56*(1), 247–265. https://doi.org/10.2307/4813
33. Oliveira, L. F. P., Moreira, A. P., & Silva, M. F. (2021). Advances in agriculture robotics: A state-of-the-art review and challenges ahead. *Robotics*, *10*(2). https://doi.org/10.3390/robotics10020052
34. Patidar, R., Chundawat, G. S., Pippal, S. S., & Tomar, S. P. S. (2023). Effect ofabiotic factors on the population dynamics of red spider mite, *Tetranychus urticae* Koch. of brinjal in Malwa region, Madhya Pradesh, India. *International Journal of Environment and Climate Change*, *13*(11), 889–895. https://doi.org/10.9734/ijecc/2023/v13i113236
35. R Core Team (2022). R: A language and environment for statistical computing. *R Foundation for Statistical Computing, Vienna, Austria*. https://www.r-project.org/

36. Rigby, R. A., & Stasinopoulos, D. M. (2005). Generalized additive models for location, scale and shape. *Journal of the Royal Statistical Society: Series C (Applied Statistics)*, *54*(3), 507–554. https://doi.org/10.1111/j.1467-9876.2005.00510.x
37. Rijal, J. P., Wilson, R., & Godfrey, L. D. (2016). Characterization of spatial distribution of *Tetranychus urticae* in peppermint in California and implication for improving sampling plan. *Experimental & Applied Acarology*, *68*(2), 155–171. https://doi.org/10.1007/s10493-015-0006-1
38. Sabelis, M. W., Janssen, A., Diekmann, O., Jansen, V. A. A., van Gool, E., & van Baalen, M. (2005). Global persistence despite local extinction in acarine predator-prey systems: Lessons from experimental and mathematical exercises. In *Advances in Ecological Research* (Vol. 37, pp. 183–220). Academic Press. https://doi.org/10.1016/S0065-2504(04)37006-6
39. Santos, J. L., Pereira, P. S., Reis, K. H. B., Freitas, D. R., Picanço Filho, M. C., Peluzio, J. M., et al. (2024). Decision-making for thrips control in soybean fields using precision agriculture principles. *Journal of Applied Entomology*, *148*(2), 140–149. https://doi.org/10.1111/jen.13215
40. Sciarretta, A., & Trematerra, P. (2014). Geostatistical tools for the study of insect spatial distribution: Practical implications in the integrated management of orchard and vineyard pests. *Plant Protection Science*, *50*(2), 97–110. https://doi.org/10.17221/40/2013-PPS
41. So, P. M. (1991). Distribution patterns of and sampling plans for *Tetranychus urticae* Koch (Acarina: Tetranychidae) on roses. *Researches on Population Ecology*, *33*(2), 229–243. https://doi.org/10.1007/BF02513551
42. Tehri, K., Gulati, R., & Geroh, M. (2014). Impact of weatherparameters on the population dynamics of *Tetranychus urticae* Koch on field grown cucumber. *Annals of Biology*, *30*(1), 140–145.
43. Tramboo, H. A., Sherwani, A., Ahmad, M. M., Khan, A. A., Malik, A. A., Jaiswal, R., & Shah, M. A. (2025). Canopy stratification, seasonal dynamics, and machine learning-based forecasting of *Tetranychus urticae* Koch on cucumber under polyhouse conditions. *Journal of Plant Diseases and Protection*, *132*(5), 138. https://doi.org/10.1007/s41348-025-01141-x
44. Van den Boom, C. E. M., van Beek, T. A., & Dicke, M. (2003). Differences among plant species in acceptance by the spider mite *Tetranychus urticae* Koch. *Journal of Applied Entomology*, *127*(3), 177–183. https://doi.org/10.1046/j.1439-0418.2003.00726.x
45. Walzer, A., Moder, K., & Schausberger, P. (2009). Spatiotemporal within-plant distribution of the spider mite *Tetranychus urticae* and associated specialist and generalist predators. *Bulletin of Entomological Research*, *99*(5), 457–466. https://doi.org/10.1017/S0007485308006494
46. Wickham, H. (2011). ggplot2. *WIREs Computational Statistics*, *3*(2), 180–185. https://doi.org/10.1002/wics.147
47. Yehoshua, A., Bechar, A., Cohen, Y., Shmuel, L., & Edan, Y. (2023). Dynamic sampling algorithm for agriculture-monitoring ground robot. *International Journal of Simulation Modelling*, *22*(3), 392–403. https://doi.org/10.2507/IJSIMM22-3-646
48. Zemek, R., & Nachman, G. (1999). Interactions in a tritrophic acarine predator– prey metapopulation system: prey location and distance moved by *Phytoseiulus persimilis* (Acari: Phytoseiidae).

Figures

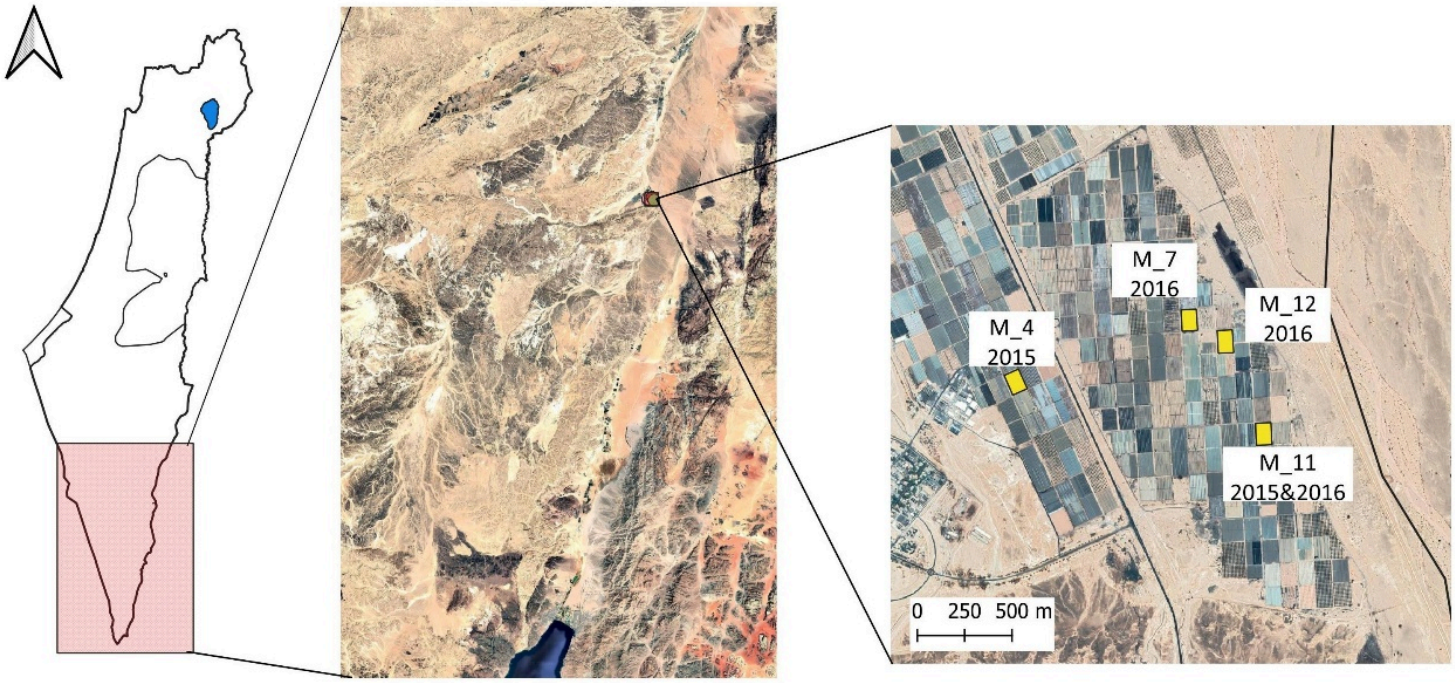


Figure 1

Study site and locations of the monitored screenhouses. (Left) Map of Israel. (Center) Enlarged view of the central Arava Valley region. (Right) Detailed map of the Paran growing area showing the locations of the sampled screenhouses, with the corresponding growing season(s) indicated for each screenhouse.

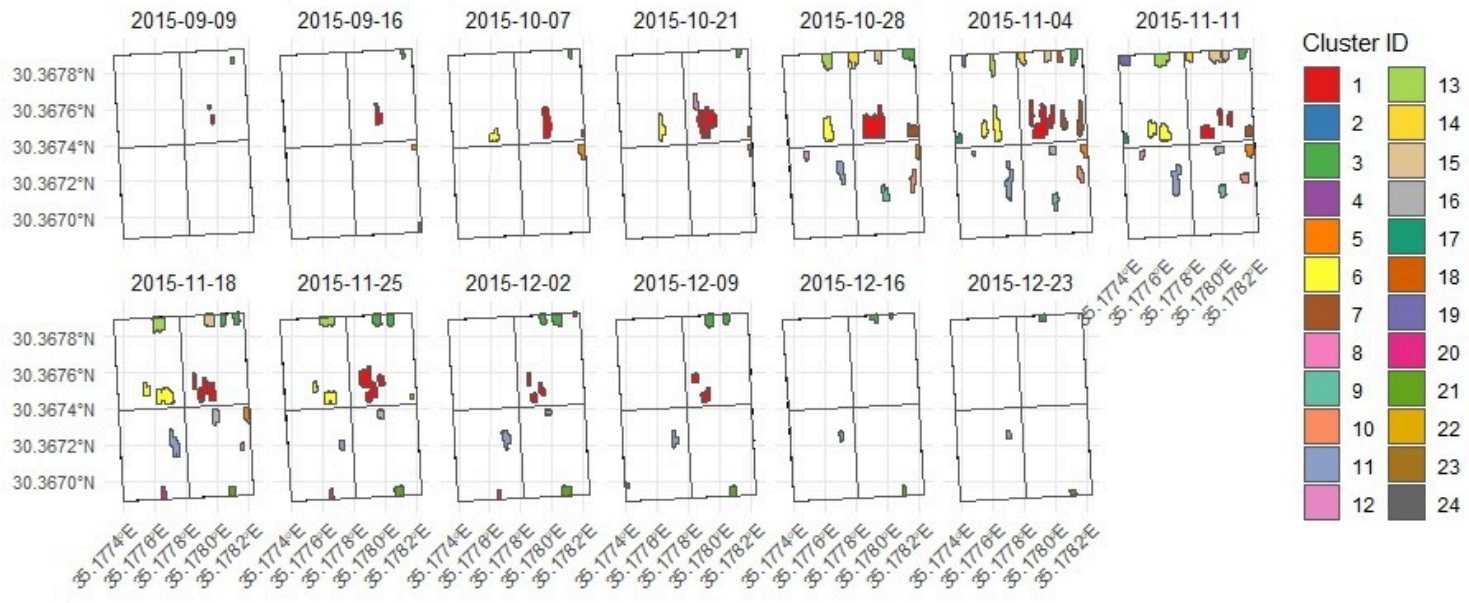


Figure 2

Tracking TSSM infestation clusters over time within screenhouse M_11 during the 2015 growing season. Each panel represents a consecutive sampling date, showing the spatial position and extent of infestation clusters. Each individual cluster is represented by a distinct identification number and color indicating its continuity across the monitoring period.

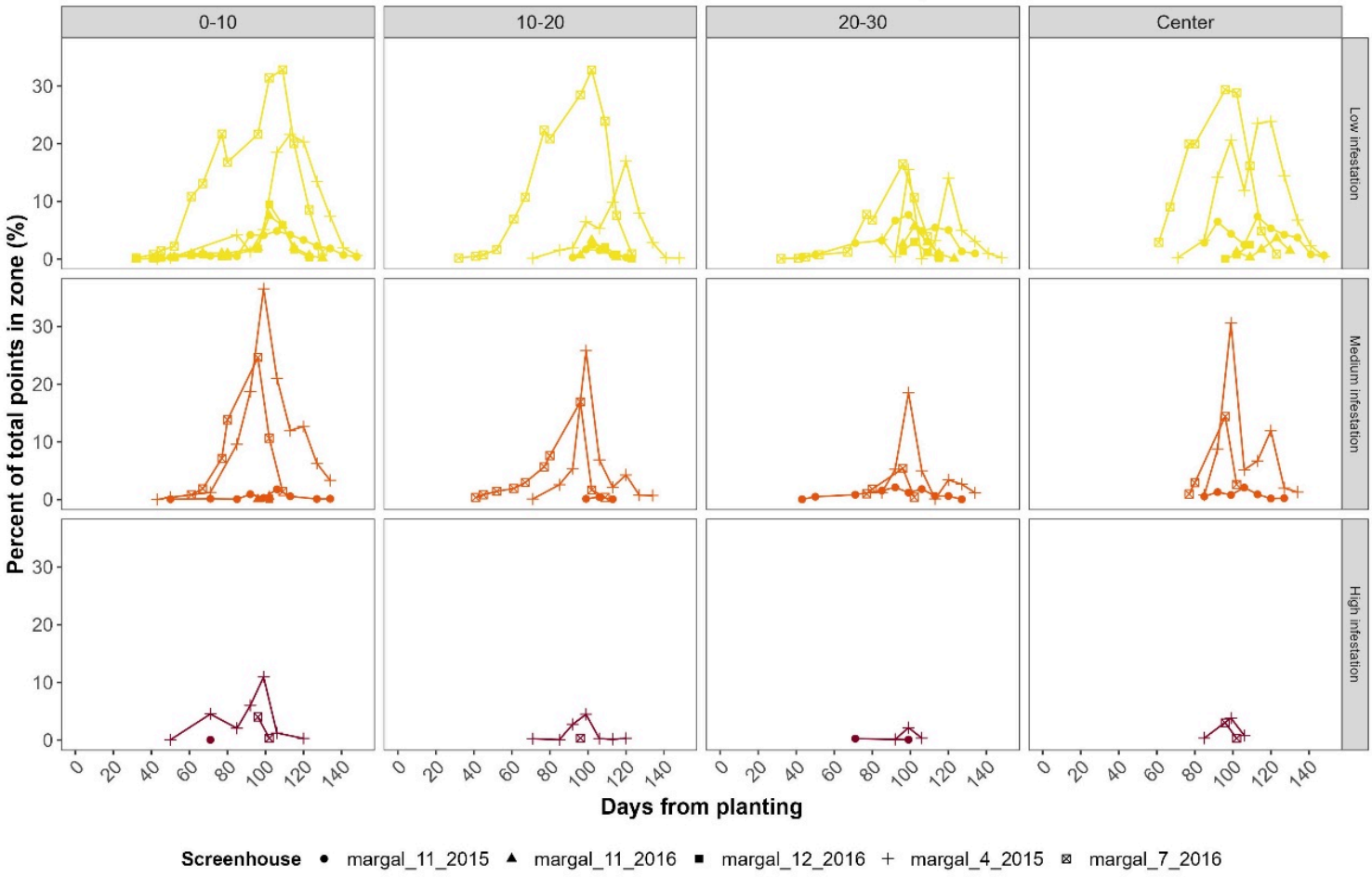


Figure 3

Temporal dynamics of TSSM infestation by distance from the screenhouse edge. Columns representing buffer zones generated at 10 m intervals from the screenhouse boundary, with an additional “center” zone representing the inner area. Rows indicate infestation severity categories: low (top), medium (middle), and high (bottom). Points show the percentage of total sampled foci over days after planting (DAP), with symbols representing different screenhouses.

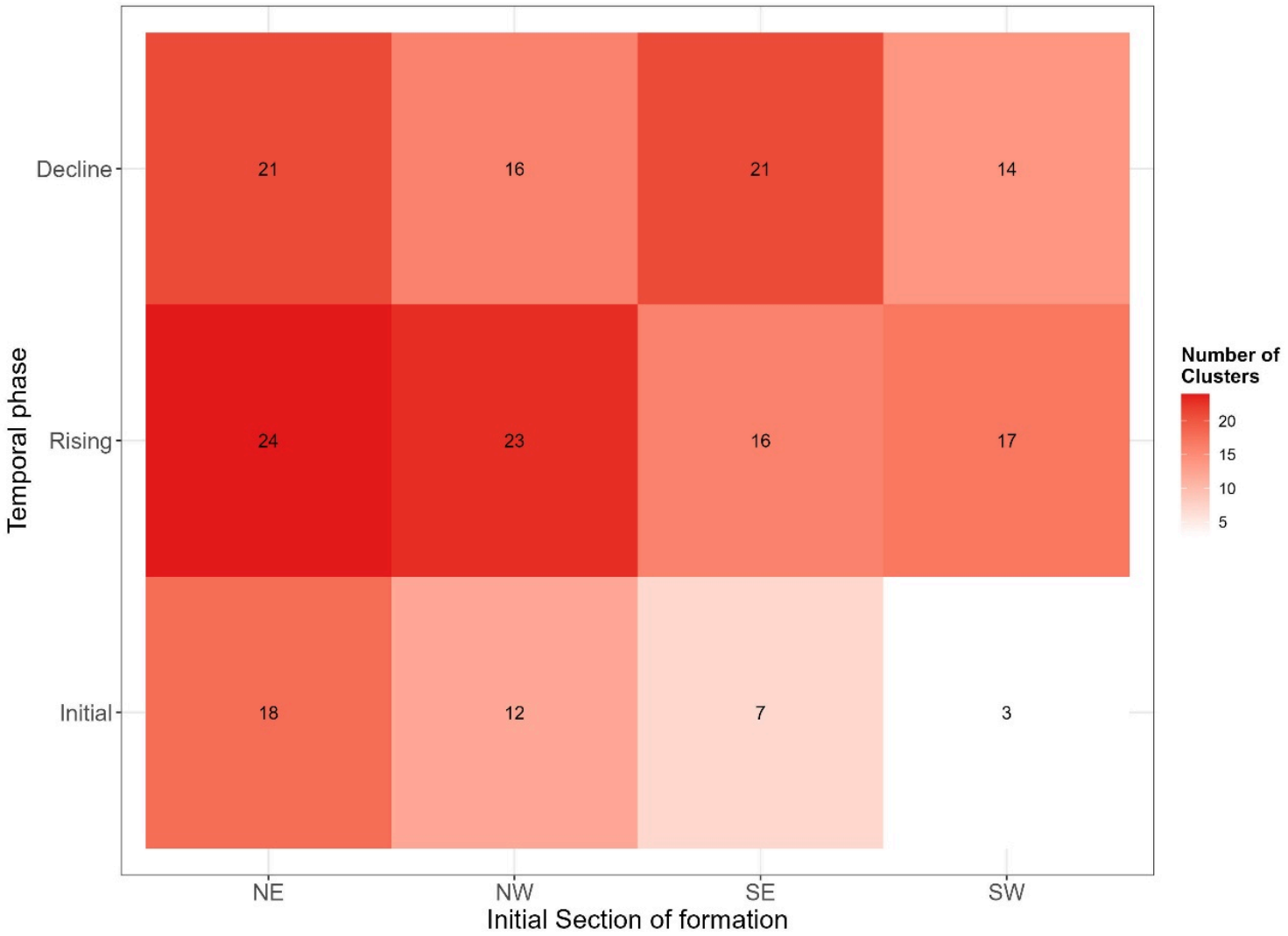


Figure 4

Heatmap showing the number of TSSM infestation clusters by temporal phase and initial section of formation within the screenhouses. Rows represent temporal phases (*Initial*, *Rising*, and *Decline*), and columns represent the screenhouse quadrants (NE, NW, SE, SW) where clusters initially appeared. Color intensity corresponds to the number of clusters in each category, with darker shades indicating higher counts.

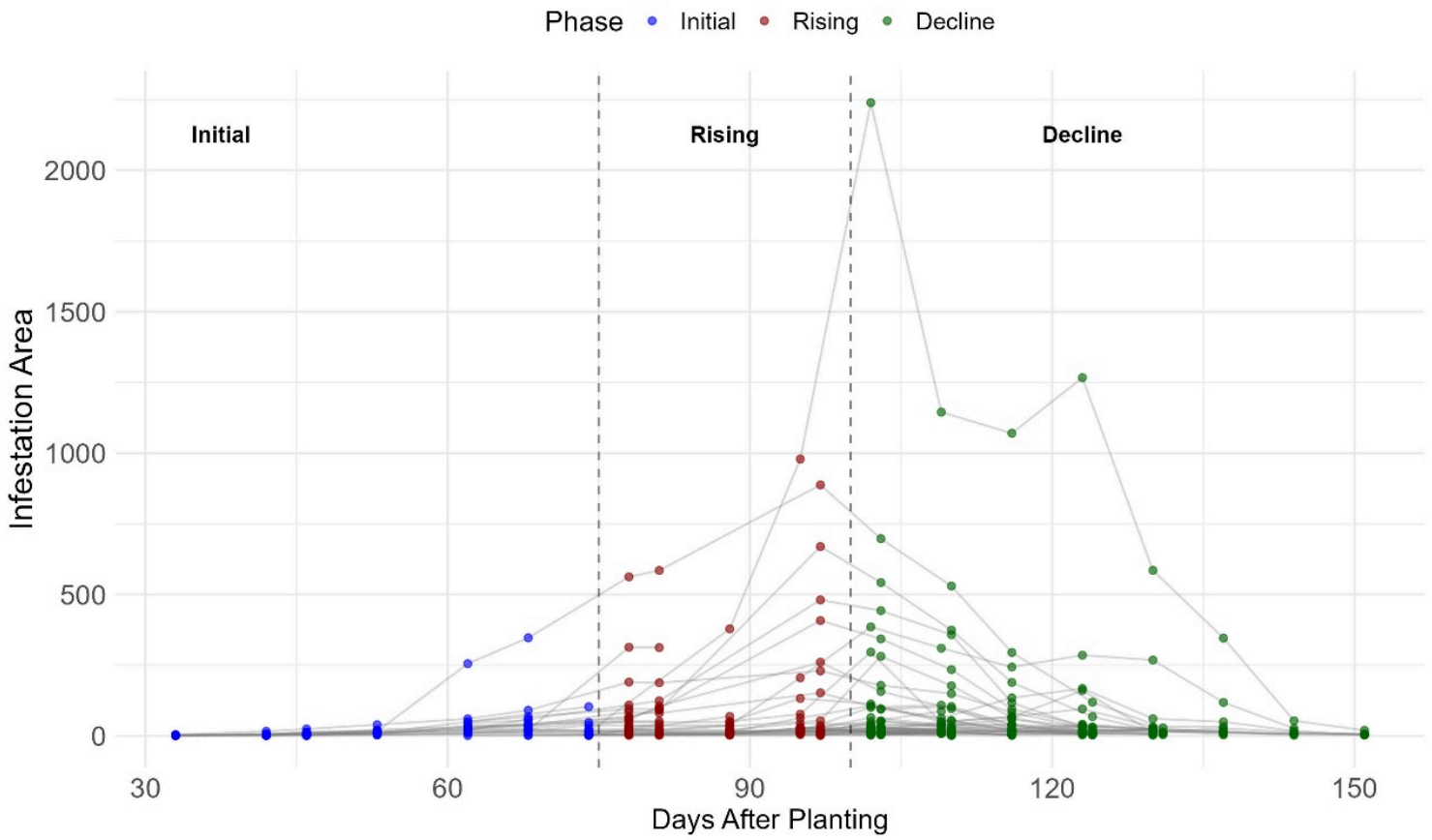


Figure 5

Area infested of each cluster by time (days after planting). Each point represents an individual cluster's area (n = 124), lines representing a single cluster tracked over time. Colors of the points indicate the temporal phase as defined in section 2.4.3: Blue – *Initial*, Red – *Rising*, and Green – *Decline*.

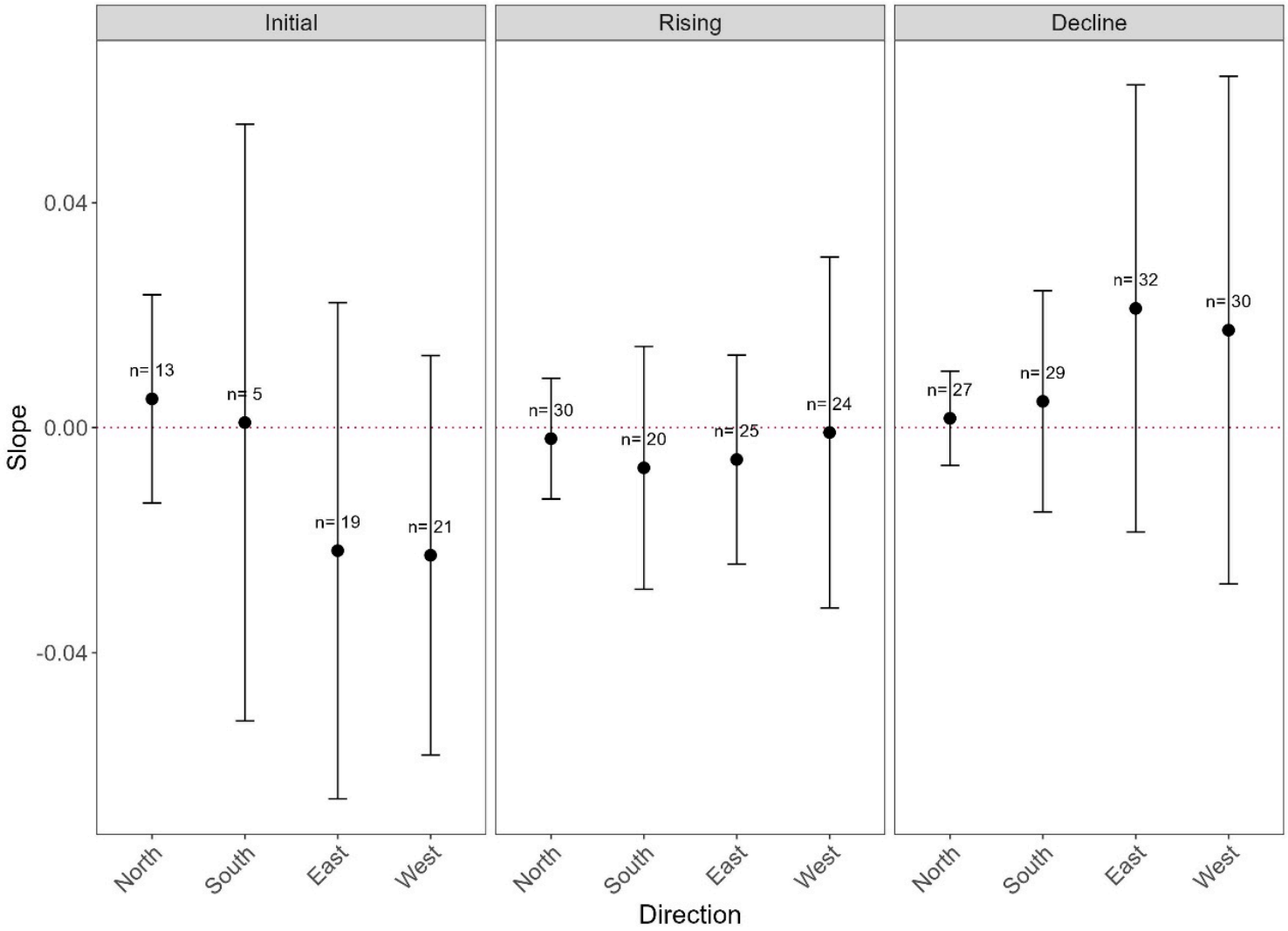


Figure 6

Mean (± SD) rates of change in the distance between TSSM infestation clusters and the screenhouse boundaries (North, South, East, and West) during the *Initial*, *Rising*, and *Decline*phases. Slopes were estimated from linear regressions of cluster-to-wall distance against time, with negative values indicating movement toward a given wall and positive values indicating movement away from it. The zero reference is indicated by a dotted line for visual guidance.

Supplementary Files

This is a list of supplementary files associated with this preprint. Click to download.

- Gafnietal2026TSSMpapersupplementary.docx